

Photon correlation measurements of stochastic limit cycles emerging from high- Q nonlinear silicon photonic crystal microcavities

N. Takemura,^{1,2,*} M. Takiguchi,^{1,2} H. Sumikura,^{1,2} E. Kuramochi,^{1,2} A. Shinya,^{1,2} and M. Notomi^{1,2}

¹NTT Nanophotonics Center, NTT Corp., 3-1, Morinosato Wakamiya Atsugi, Kanagawa 243-0198, Japan

²NTT Basic Research Laboratories, NTT Corp., 3-1, Morinosato Wakamiya Atsugi, Kanagawa 243-0198, Japan

(Dated: March 11, 2022)

We performed measurements of photon correlation $[g^{(2)}(\tau)]$ in driven nonlinear high- Q silicon (Si) photonic crystal (PhC) microcavities. The measured $g^{(2)}(\tau)$ exhibits a damped oscillatory behavior when input pump power exceeds a critical value. From comparison between experiments and simulations, we attribute the measured oscillation of $g^{(2)}(\tau)$ to self-pulsing (a limit cycle) emerging from an interplay between photon, carrier, and thermal dynamics. Namely, the oscillation frequency of $g^{(2)}(\tau)$ corresponds to the oscillation period of the limit cycle, while its finite coherence (damping) time originates from the stochastic nature of the limit cycle. From the standpoint of phase reduction theory, we interpret the measured coherence time of $g^{(2)}(\tau)$ as the coherence (diffusion) time of a generalized phase of the limit cycle. Furthermore, we show that an increase in laser input power enhances the coherence time of $g^{(2)}(\tau)$ up to the order of microseconds, which could be a demonstration of the stabilization of a stochastic limit cycle through pumping.

PACS numbers: 78.20.Ls, 42.65.-k, 76.50.+g

A limit cycle is a universal natural phenomenon observed in a variety of systems ranging from electrical circuits to biological systems. In particular, in living systems, limit cycles play fundamental roles, for example, as biochemical oscillators including a cell cycle and a circadian clock [1]. Importantly, as schematically shown on the left in Fig. 1(a), limit cycles exist only for nonlinear dissipative systems, and they are qualitatively different from periodic oscillations in conservative systems such as simple pendulums. For example, the orbit of a pendulum is determined by the initial condition and is unstable for a perturbation, whereas a limit cycle has a stable orbit, which is an attractor independent of an initial condition but controlled by system parameters such as pump power. At the same time, dissipative systems are usually noisy environments. Therefore, biochemical oscillators work as stochastic limit cycles, and strategies to maintain the precision of stochastic biochemical oscillators have been actively investigated in theoretical biophysics and biochemistry [2–8]. In this direction, a novel strategy is to increase the amplitude of a limit cycle [2, 3], which can be achieved by pumping [4] or by free-energy dissipation [5, 7].

In this paper, we report experimental investigations of stochastic limit cycles in the optical domain and demonstrate a strategy for stabilizing a stochastic limit cycle with pumping. Our system is based on a driven silicon (Si) photonic crystal (PhC) high- Q microcavity. A photonic microcavity device confines photons inside a nanoscale mode volume, which strongly enhances thermo-optic (TO) and carrier-induced optical nonlinearities in a medium such as a III-V material and Si [9–11]. Using the enhanced optical nonlinearity, optical bistability has been demonstrated with microcavities [12–17]. Fur-

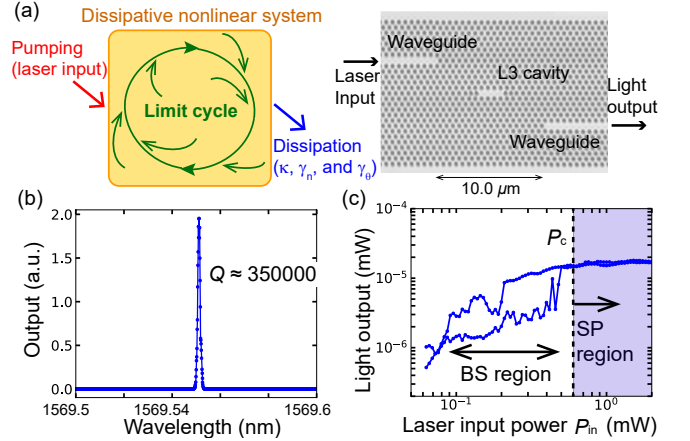


FIG. 1. (a) Illustration of a limit cycle emerging from a driven dissipative nonlinear system (left) and a laser scanning microscope image of the high- Q Si PhC microcavity (right). (b) A laser transmission spectrum of the cavity shows the resonance of a fundamental mode. (c) Output intensity I_{out} as a function of input power P_{in} , where P_c is the critical laser input power of self-pulsing. BS and SP represent bistable and self-pulsing regions, respectively. In this paper, P_{in} is the fiber output power of the tunable semiconductor laser.

thermore, it is known that nonlinear photonic microcavities exhibit Hopf bifurcation, self-pulsing (a limit cycle) [18–22], and excitability [23, 24]. Advantages of using a photonic system are its good controllability, such as controllability of pump (laser input) power, and easiness of measurements, such as photon correlation measurements. In fact, in our study, we measured second-order photon correlation functions $[g^{(2)}(\tau)]$ for a light output of the driven cavity. When laser input power exceeded a critical value, $g^{(2)}(\tau)$ exhibited damped oscillation. Together with numerical simulations, we show that the origin of

the oscillation of $g^{(2)}(\tau)$ is self-pulsing (a limit cycle). Next, we argue that the finite coherence time of $g^{(2)}(\tau)$ originates from the stochastic nature of the system. The coherence time of $g^{(2)}(\tau)$ is interpreted as the coherence (diffusion) time of the generalized phase of the limit cycle [25, 26]. Measuring the input power dependence of the coherence time of $g^{(2)}(\tau)$, we observed an enhancement of the phase coherence time up to the order of microseconds with an increase in input power. Finally, we discuss the observed enhancement of the phase coherence time as a general property of a limit cycle, namely as a demonstration of stabilization of a stochastic limit cycle through pumping [2–4, 8].

On right in Fig. 1(a) is an image of our device, which is based on a 2D Si PhC slab with a cavity and two waveguides. The lattice constant, air hole radius, and thickness of the PhC slab are 412, 200, and 215 nm, respectively. The cavity resonance of the fundamental mode is $\lambda_c = 1569.55$ nm, and the Q value is around 3.5×10^5 [see Fig. 1(b)]. The corresponding cavity photon lifetime is around 300 ps. This very high Q value is achieved by the ultrahigh- Q design proposed in Ref. [27], which omits three air holes and employ careful modulation of surrounding air holes. We drive the cavity through the input waveguide with a tunable semiconductor laser, while we measure light outputs through the output waveguide. We introduce a normalized frequency detuning δ between the cavity resonance and laser input, which is defined as $\delta = (\omega_L - \omega_c)/\kappa$ with the cavity resonance frequency ω_c , the laser input frequency ω_L , and a field decay rate κ . In the measurements, we fixed the detuning as $\delta \simeq -2$. To measure second-order photon correlation functions $[g^{(2)}(\tau)]$, we employed single-photon detectors (SSPDs) and a conventional start-stop Hanbury brown-Twiss (HBT) interferometer. For real-time measurements, we use an avalanche photodiode (APD).

First, we discuss bistable operation shown in Fig. 1(c). When the detuning is $\delta \simeq -2$, the light output intensity I_{out} exhibits a hysteresis loop in terms of laser input power P_{in} . We use a negative detuning ($\delta \simeq -2$) to induce the TO nonlinearity. The hysteresis loop shown in Fig. 1(c) is very noisy, which is probably because we performed a single shot measurement by up and down laser input power ramping slowly enough to induce the TO nonlinearity. The lower and upper thresholds of the bistable hysteresis loop are about $P_{\text{in}} = 0.08$ and 0.5 mW, respectively. Note that the laser input power P_{in} was measured as the fiber output of the tunable semiconductor laser. If the coupling loss from the fiber output and to the input waveguide is assumed to be 10 dB, the lower threshold power of bistability is 8 μ W in the input waveguide, which is as low as those reported in our previous experiments [13, 28]. Thus, the bistable operation in Fig. 1(c) is evidence of the onset of a high- Q cavity-enhanced optical nonlinearity induced by a very small input power.

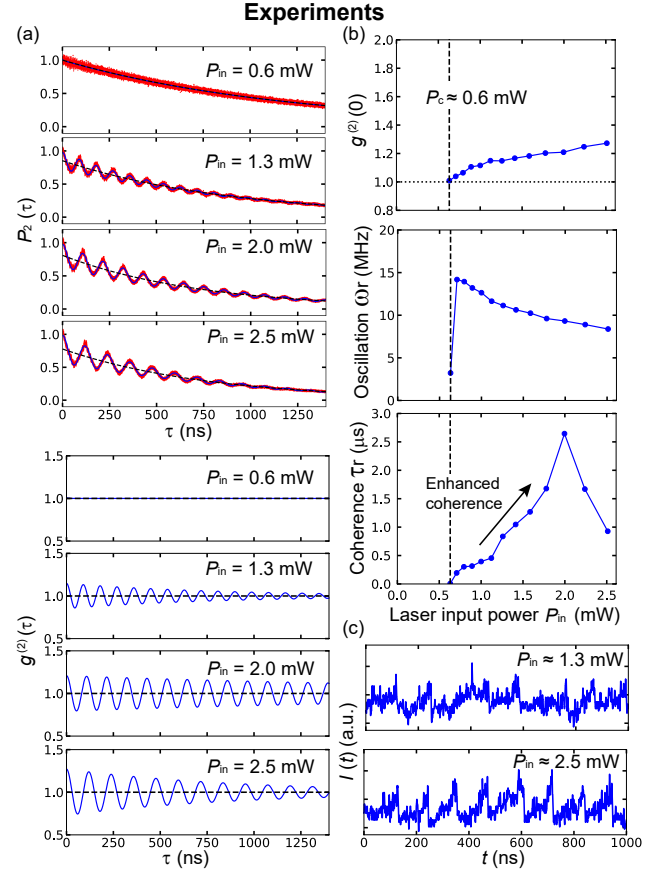


FIG. 2. (a) Examples of measured photon correlations with the start-stop HBT interferometer $P_2(\tau)$ with a fitting curve by Eq. (1) and reconstructed normalized second-order photon correlation functions $g^{(2)}(\tau)$. (b) $g^{(2)}(0)$ (top), the oscillation frequency ω_r (middle), and the coherence time τ_r (bottom) of measured $g^{(2)}(\tau)$. The critical input power of self-pulsing is $P_c \simeq 0.6$ mW. (c) Real-time trajectories of the light output measured with an avalanche photodiode (APD) for two pump powers. For measurements, the detuning was fixed as $\delta \simeq -2$.

Second, for various laser input powers P_{in} , we measured the delay-dependent photon correlations $P_2(\tau)$ with the start-stop HBT interferometer, and attempted to reconstruct the normalized second-order photon correlation $g^{(2)}(\tau)$ from $P_2(\tau)$. $P_2(\tau)$ is a histogram of detecting photon pairs in terms of the time delay τ . The upper part of Fig 2(a) shows $P_2(\tau)$ for four laser input powers. The overall exponential decay of the measured $P_2(\tau)$ is a well-known artifact associated with the start-stop measurement [29]. Namely, when τ is longer, the probability to detect photon pairs becomes smaller. Now, we define $g^{(2)}(\tau)$ as a classical intensity correlation $g^{(2)}(\tau) \equiv \langle I(t)I(t+\tau) \rangle / \langle I \rangle^2$, where the brackets represent statistical averages. For reconstructing normalized second-order photon correlation functions $g^{(2)}(\tau)$, we fit measured $P_2(\tau)$ as

$$P_2(\tau) \simeq C \left[1 + A e^{-\frac{|\tau|}{\tau_r}} \cos(\omega_r |\tau|) \right] e^{-\frac{\tau}{\tau_{\text{cor}}}}, \quad (1)$$

where $A \equiv g^{(2)}(0) - 1$, and C is another fitting parameter. Additionally, ω_r and τ_r are the oscillation frequency and coherence (damping) time of $g^{(2)}(\tau)$, respectively. On the other hand, τ_{cor} is the overall decay time of $P_2(\tau)$ associated with the start-stop counting method. With this fitting, we reconstruct $g^{(2)}(\tau)$ as $g^{(2)}(\tau) = g^{(2)}(0) \cos(\omega_r |\tau|) e^{-\tau/\tau_r}$. In the lower part of Fig. 2(a), we show four reconstructed $g^{(2)}(\tau)$ corresponding to the four $P_2(\tau)$. When laser input power is below a critical value, and even when input power is in the bistable hysteresis loop, the light output has a Poissonian fluctuation, and thus $g^{(2)}(\tau) = 1$ as shown in Fig. 2(a) for $P_{\text{in}} = 0.6$ mW. Meanwhile, when laser input power is above the critical value, $g^{(2)}(0)$ deviates from unity and $g^{(2)}(\tau)$ exhibits damped oscillation [see $P_{\text{in}} = 1.3$ mW in Fig. 2(a)]. The critical laser input power of damped oscillation of $g^{(2)}(\tau)$ was measured as $P_c \simeq 0.6$ mW, which is above the hysteresis loop as shown in Fig. 1(c). In Fig. 2(b), we plot the second-order photon correlation at a zero delay time $g^{(2)}(0)$ (top), the oscillation frequency ω_r (middle), and the coherence time τ_r (bottom) of $g^{(2)}(\tau)$. Figure 2(b) clearly shows that $g^{(2)}(0)$ deviates from unity when $P_{\text{in}} = P_c$. Additionally, the oscillation frequency ω_r has a maximum ($\omega_r = 14$ MHz) when $P_{\text{in}} = P_c$, and it gradually decreases with an increase in laser input power. Meanwhile, for the coherence time τ_r , above P_c , τ_r increases with an increase in laser input power (indicated by an arrow) and reaches a maximum value of $2.6 \mu\text{s}$ when $P_{\text{in}} \simeq 2.0$. However, when laser input power is increased further, the coherence time τ_r starts to decrease with an increase in laser input power.

We attribute the origin of the oscillation of $g^{(2)}(\tau)$ to self-pulsation (a limit cycle) originating from Hopf bifurcation [18–20, 22–24]. To confirm this, we performed real-time measurements of the light output. Figure 2(c) shows real-time trajectories of light outputs measured with the APD for two input powers above P_c , which clearly indicates real-time self-pulsation. Thus, here the origin of photon bunching [$g^{(2)}(0) > 1$] is the real-time modulation of light intensity [30], which is different from the photon bunching mechanism of chaotic light.

Now, a new question arises: What is the origin of the finite coherence time of the observed $g^{(2)}(\tau)$? The answer is the stochastic (noisy) nature of our limit cycle. In fact, without any noise, $g^{(2)}(\tau)$ will never decay and should have an infinite coherence time. For a deeper understanding of these experimental results, we performed numerical simulations based on coupled-mode equations proposed in Ref. [17, 31, 32]. Neglecting the Kerr effects, the normalized coupled-mode equations for an electric field α , normalized carrier density n , and thermal effect θ are given by

$$\dot{\alpha} = \kappa \{i(-\delta - \theta + n) - (1 + fn)\} \alpha + \kappa \sqrt{P_{\text{in}}} \quad (2)$$

$$\dot{n} = \gamma_n \{-n + \xi |\alpha|^4\} \quad (3)$$

$$\dot{\theta} = \gamma_\theta \{-\theta + \beta |\alpha|^2 + \eta |\alpha|^2 n\}. \quad (4)$$

Here, θ is proportional to the temperature difference between in the cavity and in the surrounding region [31]. Both n and θ are normalized to make constants of nonlinear energy shifts in Eq. (2) unity. The κ , γ_n , and γ_θ are decay rates of the electric field, the carrier, and the thermal effect, respectively. P_{in} represents normalized laser input power. The coefficients f , ξ , β , and η represent nonlinear effects associated with free-carrier absorption (FCA), two-photon absorption (TPA), heating with linear photon absorption, and FCA-induced heating, respectively. For these nonlinear coefficients, we use the same values as in Ref. [32]: $f = 0.0244$, $\xi = 8.2\kappa/\gamma_n$, $\beta = 0.0296\kappa/\gamma_\theta$, and $\eta = 0.0036\kappa/\gamma_\theta$. For the photon, carrier, and thermal lifetimes, we use $1/2\kappa = 300$ ps, $1/\gamma_n = 200$ ps, and $1/\gamma_\theta = 100$ ns, respectively. The fast carrier lifetime ($1/\gamma_n = 200$ ps) results from fast carrier diffusion associated with the small cavity of the PhC structure [12, 33].

Before showing the simulated dynamical properties, we briefly investigate static properties of the coupled-mode equations (2)-(4). We attempt to obtain steady state values of α , n , and θ , which are denoted as α_s , n_s , and θ_s , respectively. By putting $\dot{\alpha} = 0$, $\dot{n} = 0$, and $\dot{\theta} = 0$ into Eqs. (2)-(4), we obtain an algebraic equation for $I_s = |\alpha_s|^2$:

$$P_{\text{in}} = I_s [(-\delta - \beta I_s - \eta \xi I_s^3 + \xi I_s^2)^2 + (1 + f \xi I_s^2)^2]. \quad (5)$$

The system is bistable when Eq. (5) has two solutions for I_s . For various laser input power P_{in} and detuning δ values, we numerically solved Eq. (5) and obtained I_s . With I_s , the steady-state carrier number n_s , thermal component θ_s , and complex electric field α_s are easily calculated. At the steady state values of α_s , n_s , and θ_s , we calculate a Jacobian matrix and its eigenstates to find self-pulsing. Since α is decomposed as $\alpha = \alpha_x + i\alpha_y$, the Jacobian is a 4×4 matrix. When the eigenvalues of the Jacobian have positive real parts, the dynamical system becomes unstable and self-pulsing occurs (Hopf bifurcation). A diagram of the dynamical system described by coupled-mode equations (2)-(4) is shown in Fig. 3(a), where the colored regions labeled BS and SP represent bistable and self-pulsing regions, respectively. The fact that the BS and SP regions are located in the negative detuning indicates that the TO nonlinearity is relevant to both phenomena. More precisely, bistability (BS) is induced solely by TO nonlinearity, while self-pulsing requires both carrier and TO nonlinearities. The horizontal dashed line in Fig. 3(a) indicates that, for $\delta = -2$, with an increase in pump power, self-pulsing occurs above the bistable region. This is consistent with our measurement shown in Fig. 1(c). Furthermore, we find that as photon lifetime increases (a Q value increases), the SP region separates from the BS region and self-pulsing occurs

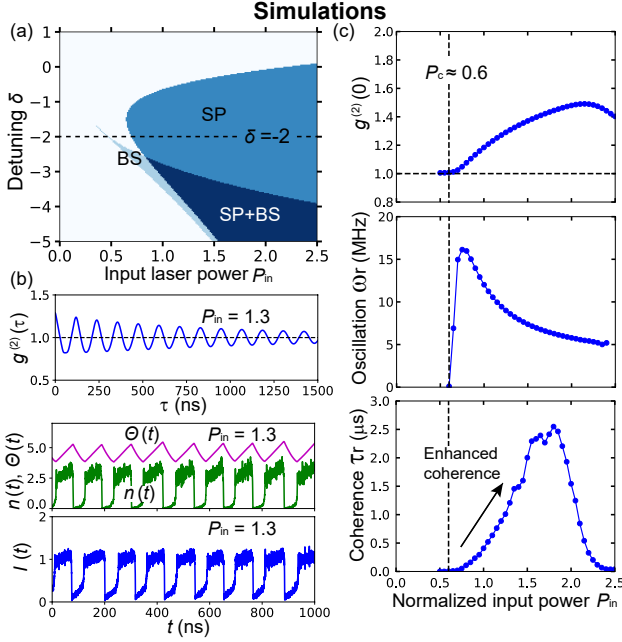


FIG. 3. (a) Simulated self-pulsing (SP) and bistable (BS) regions as a map of detuning δ and laser input power P_{in} . (b) Simulated $g^{(2)}(\tau)$ and real-time evolution of carrier $n(t)$, thermal effect $\theta(t)$, and the light output $I(t) = |\alpha(t)|^2$ for $P_{in} = 1.3$. (c) $g^{(2)}(0)$ (top), oscillation frequencies ω_r (middle), and the coherence time τ_r (bottom) of the simulated $g^{(2)}(\tau)$. For simulations, the detuning $\delta = -2$ is used. The critical input power of self-pulsing is $P_c = 0.6$. While (a) is the result with the deterministic coupled-mode equations, (b) and (c) are the results with stochastic coupled-mode equations with noise terms.

with a near-zero detuning and low input power. In fact, in our experiment, we were able to observe self-pulsing outside the hysteresis loop with moderate negative detuning ($\delta \simeq -2$) and low input power ($P_c \simeq 0.6$ mW). Thus, high Q value will be technically very important for observation of self-pulsing. Furthermore, when Q is reduced to around 2.0×10^4 , we will not be able to investigate self-pulsing around bifurcation due to a large overlap between the BS and SP regions. A detailed discussion of the impact of Q on self-pulsing is given in the Supplemental Material.

Now, we investigate the dynamical properties of coupled-mode equations (2)-(4). Since we are interested in a fluctuating system, we add additive Langevin noises f_x and f_y only to Eq (4), where we assume that field and laser input noises are dominant over other noises. Actually, we find that inclusion of carrier and thermal noises does not qualitatively modify the results. The noise terms satisfy correlations $\langle f_i(t)f_j(t') \rangle = 2D\delta_{ij}\delta(t-t')$ and $\langle f_i(t) \rangle = 0$, where $i(j) = x, y$ and the coefficient, D , is the strength of the noise. For numerical simulations of the stochastic equations, we employed the Euler-Maruyama method. The value of the noise strength was set as $\sqrt{2D} = 0.045\sqrt{\kappa}$, which was chosen to repro-

duce the observed maximum coherence time of $g^{(2)}(\tau)$ [34]. Figure 3(b) shows simulated $g^{(2)}(\tau)$, $n(t)$, $\theta(t)$, and $I(t) = |\alpha(t)|^2$ for input power $P_{in} = 1.3$, which clearly reproduce the damped oscillatory behavior of $g^{(2)}(\tau)$ and the real-time self-pulsing when the input power is above the critical input power $P_c = 0.6$. Additionally, in Fig. 3(c), we plot $g^{(2)}(0)$ (top), the oscillation frequency ω_r (middle), and the coherence time τ_r (bottom) of $g^{(2)}(\tau)$ as a function of P_{in} , which also qualitatively reproduce the measurements shown in Fig. 2(b). Namely, the simulation reproduces the monotonic decrease of ω_r with an increase in pump power and the enhancement and reduction of the coherence time τ_r with an increase in pump power. Here, we briefly comment on the reduction of the coherence time τ_r in the region of high laser input power when $P_{in} > 2.0$ mW in the experiment. We notice that a certain enhancement or multiplication of noises occurs and the simulation reproduces the coherence reduction in the high input power region only when we add noise terms to α . Thus, the coherence reduction depends on a model and is not a universal property of a limit cycle.

In the rest of this paper, we focus on the region around the critical input power of self-pulsing and attempt to interpret the enhancement of the coherence time τ_r , which is indicated by an arrow in the bottom graphs of Fig. 2(b) (experiment) and Fig. 3(c) (simulation). For this purpose, a theoretical idea called “phase reduction” proposed by Winfree and Kuramoto [25, 26] plays a key role. The main idea of the phase reduction theory is that a high-dimensional limit cycle is reduced to one-dimensional dynamics on a generalized phase, ϕ , along an orbit of a limit cycle. Importantly, in the phase reduction, noises in a limit cycle are reduced to a frequency drift and a phase noise as $\dot{\phi} = \omega + v + f_\phi$, where ω , v , and f_ϕ represent the original frequency of a limit cycle, the frequency drift, and the phase noise, respectively [25, 26]. The phase noise f_ϕ satisfies correlations $\langle f_\phi(t)f_\phi(t') \rangle = 2D_\phi\delta(t-t')$ and $\langle f_\phi(t) \rangle = 0$, where D_ϕ is the phase diffusion rate. Therefore, for a limit cycle, noises are interpreted as diffusion of the generalized phase. Furthermore, the coherence time of a correlation function such as $g^{(2)}(\tau)$ corresponds to the coherence (diffusion) time of the generalized phase: $\tau_r \simeq 1/D_\phi$ [5, 7].

To be more concrete, let us recall the fact that for the stochastic Stuart-Landau model without phase-amplitude coupling, the phase diffusion rate well above Hopf bifurcation is approximated as [5, 7, 35–37]

$$D_\phi \propto D_0/P_{in}, \quad (6)$$

where D_0 is the strength of noise, while P_{in} represents the pump or input power to the system. If D_0 is constant, Eq (6) represents suppression of phase diffusion by pumping [38]. Additionally, Ref. [5] shows that Eq. (6) can also be written with a free-energy dissipation rate ΔW as $D_\phi \propto \Delta W^{-1}$, which means suppression of phase

diffusion through free-energy dissipation. Furthermore, Eq (6) is intuitively understood as a one-dimensional diffusion process along an orbit of a limit cycle [39]. Thus, if the noise strength D_0 is constant, the longer the orbit's circumference, the longer the time required for the phase to diffuse over 2π . Additionally, the amplitude and the circumference length generally increase with pumping P_{in} in the vicinity of Hopf bifurcation. Thus, the essence of Eq. (6) lies in the fixed strength of noises and the increase in the amplitude by pumping. In particular, the latter is possible only for limit cycles. Thus, in the vicinity of a critical point of self-pulsing, an enhancement of phase coherence will generally occur for any limit cycle, including ours.

In summary, we performed photon correlation measurements of stochastic limit cycles using a driven high- Q silicon photonic crystal cavity. We observed damped oscillation of photon correlation associated with self-pulsing (a limit cycle). Furthermore, by increasing input power, the coherence time of the photon correlation function was enhanced up to the order of microseconds, which could be interpreted as coherence time enhancement of a generalized phase through pumping.

Note. During preparation of the manuscript, we noticed a paper with similar keywords [40]

ACKNOWLEDGEMENTS

We thank K. Nozaki for helpful discussions.

SUPPLEMENTAL MATERIAL

In this supplemental material, we discuss the bistable behavior and self-pulsing of a Si PhC microcavity with a moderate Q value. For instance, let us consider a conventional L3 cavity without careful modulation of air holes, where the photon lifetime is much shorter than the carrier and thermal lifetimes: $\kappa \gg \gamma_n, \gamma_\theta$. Here, we set the photon lifetime as $1/2\kappa = 1/2\kappa_L = 15$ ps, which corresponds to $Q \simeq 2.0 \times 10^4$. The other lifetimes and the nonlinear coefficients are the same as in the main text. Namely, the carrier and thermal lifetimes are $1/\gamma_n = 200$ ps and $1/\gamma_\theta = 100$ ns, respectively. For the coefficients associated with optical nonlinearities, we set $f = 0.0244$, $\xi = 8.2\kappa/\gamma_n$, $\beta = 0.0296\kappa/\gamma_\theta$, and $\eta = 0.0036\kappa/\gamma_\theta$.

First, we investigate the static properties as we did in the main text. In Fig. 4(a), we present the regions of bistability (BS) and self-pulsing (SP) as functions of the detuning δ and a scaled input power \tilde{P}_{in} . Here, the detuning δ is defined with κ_L as $\delta = (\omega_L - \omega_c)/\kappa_L$. Meanwhile, input power P_{in} is scaled as $\tilde{P}_{\text{in}} \equiv (\kappa_L/\kappa_H)^2 P_{\text{in}}$ with $1/2\kappa_H = 300$ ps for direct comparison with the input power in Fig. 3 (a) in the main text. Actually,

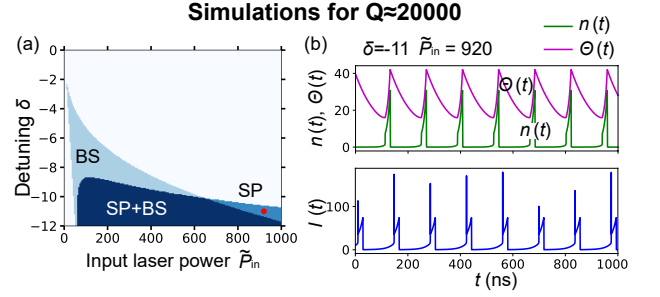


FIG. 4. Simulations for a Si PhC cavity with the photon lifetime of $1/2\kappa = 15$ ps with the deterministic equations (8) and (8). (a) Self-pulsing (SP) and bistable (BS) regions as functions of detuning δ and scaled laser input power $\tilde{P}_{\text{in}} \equiv (\kappa_L/\kappa_H)^2 P_{\text{in}}$, where $1/2\kappa_L = 15$ ps and $1/2\kappa_H = 300$ ps. (b) Real-time evolution of carrier $n(t)$, thermal effect $\theta(t)$, and light output $I(t) = |\alpha(t)|^2$ for $\delta = -11$ and $\tilde{P}_{\text{in}} = 920$. For simulations, we used the same parameters as in Fig. 3 in the main text except for the photon lifetime.

$1/2\kappa_H = 300$ ps is the photon lifetime used for simulations in the main text. Figure 4(a) indicates that when the Q value is decreased to around 2.0×10^4 , the self-pulsing (SP) region shifts to a large negative detuning and largely overlaps the bistable (BS) region [See the SP+BS region in Fig. 4(a)]. In the overlap (SP+BS) region, self-pulsing occurs only in the upper (brighter) state of a hysteresis, which is achieved only by careful up and down ramping of input power without noises. Thus, in the real world, we may not be able to observe self-pulsing in the overlap (SP+BS) region. Therefore, to purely observe self-pulsing, we should use the SP region, where the detuning has a large negative value and input power is larger than the upper threshold of bistability. To observe self-pulsing, for example, let us choose the detuning of $\delta = -11$ and input power $\tilde{P}_{\text{in}} = 920$ ($P_{\text{in}} = 2.3$), which are indicated by the filled circle in Fig. 4(a). This input power ($\tilde{P}_{\text{in}} = 920$) is a thousand times larger than the critical input power of self-pulsing in Fig. 3 in the main text and may correspond to the order of 10 mW as waveguide input power. Therefore, a higher Q value dramatically reduces not only the threshold input power of bistability but also the critical input power of self-pulsing. Furthermore, since the critical point of the self-pulsing region is overlapped with bistability [See the interface between BS and SP+BS region in Fig. 4(a)], we cannot investigate the properties of limit cycle oscillation around bifurcation points, which is the main objective of our paper.

Second, we simulated time evolutions of self-pulsing in the Si PhC microcavity with the moderate Q value. We find that the large time scale difference $\kappa \gg \gamma_n \gg \gamma_\theta$ makes direct numerical integration of coupled-mode Eqs. (2)-(4) in the main text extremely unstable. Thus, in the same way as in Ref. [31], we perform adiabatic elimination of the field degree of freedom. Putting $\dot{\alpha} = 0$

into Eq. (2) in the main text, we obtain

$$\alpha = \frac{\sqrt{P_{\text{in}}}}{\kappa} \cdot \frac{(1 + fn) + i(-\delta - \theta + n)}{(-\delta - \theta + n)^2 + (1 + fn)^2}. \quad (7)$$

Substituting Eq. (7) into Eqs. (3) and (4) in the main text, the coupled mode equations are reduced to carrier-thermal dynamics as

$$\begin{aligned} \dot{n} &= \gamma_n \left[-n + \left\{ \frac{qp}{(1 + fn)^2 + (-\delta - \theta + n)^2} \right\}^2 \right] \\ \dot{\theta} &= \gamma_\theta \left[-\theta + \frac{(1 + en)p}{(1 + fn)^2 + (-\delta - \theta + n)^2} \right], \end{aligned} \quad (8)$$

where we define $p \equiv \beta|\alpha_{\text{in}}|^2\kappa^{-2}$, $e \equiv \eta/\beta$, and $q \equiv \sqrt{\xi}/\beta$ similarly to Ref. [31]. With simulated $n(t)$ and $\theta(t)$, the electric field $\alpha(t)$ is easily calculated through Eq. (7). Since the objective of this supplementary material is not a detailed study of stochastic limit cycles, we do not add noises to Eqs. (8) and (8). Figure 4(b) shows the time evolution of $n(t)$, $\theta(t)$, and $I(t) = |\alpha(t)|^2$ for $\delta = -10$ and $\tilde{P}_{\text{in}} = 920$ ($P_{\text{in}} = 2.3$), which clearly exhibits self-pulsing (a limit cycle) with a frequency of 7.3 Hz. Interestingly, the temporal behavior of self-pulsing light output $I(t)$ shown in Fig 4(b) is more intermittent than that shown in Fig. 3 (b) in the main text, and may resemble that reported in Ref. [24].

In conclusion, simulations were performed for a Si PhC cavity with a moderate $Q \sim 2.0 \times 10^4$. The simulations indicate that a large negative detuning and high pump power are required to observe self-pulsing in a device with a moderate Q . In fact, the critical input power of self-pulsing is found to be a hundred times higher than the measured device with a high $Q \sim 3.5 \times 10^5$. Therefore, as we briefly explained in the main text, a high Q value is technically very important for observing of self-pulsing with a moderate detuning and low input power.

* E-mail: naotomo.takemura.ws@hco.ntt.co.jp

- [1] B. Novák and J. J. Tyson, *Nature Reviews Molecular Cell Biology* **9**, 981 (2008).
- [2] P. Gaspard, *The Journal of Chemical Physics* **117**, 8905 (2002), <https://doi.org/10.1063/1.1513461>.
- [3] D. Gonze, J. Halloy, and P. Gaspard, *The Journal of Chemical Physics* **116**, 10997 (2002), <https://doi.org/10.1063/1.1475765>.
- [4] H. Qian, *The Journal of Physical Chemistry B* **110**, 15063 (2006).
- [5] Y. Cao, H. Wang, Q. Ouyang, and Y. Tu, *Nature Physics* **11**, 772 EP (2015), article.
- [6] A. C. Barato and U. Seifert, *Phys. Rev. X* **6**, 041053 (2016).
- [7] C. Fei, Y. Cao, Q. Ouyang, and Y. Tu, *Nature Communications* **9**, 1434 (2018).
- [8] B. Nguyen, U. Seifert, and A. C. Barato, *The Journal of Chemical Physics* **149**, 045101 (2018), <https://doi.org/10.1063/1.5032104>.

- [9] P. E. Barclay, K. Srinivasan, and O. Painter, *Opt. Express* **13**, 801 (2005).
- [10] T. Uesugi, B.-S. Song, T. Asano, and S. Noda, *Opt. Express* **14**, 377 (2006).
- [11] J. Leuthold, C. Koos, and W. Freude, *Nature Photonics* **4**, 535 EP (2010), review Article.
- [12] T. Tanabe, M. Notomi, S. Mitsugi, A. Shinya, and E. Kuramochi, *Opt. Lett.* **30**, 2575 (2005).
- [13] M. Notomi, A. Shinya, S. Mitsugi, G. Kira, E. Kuramochi, and T. Tanabe, *Opt. Express* **13**, 2678 (2005).
- [14] T. Tanabe, A. Shinya, E. Kuramochi, S. Kondo, H. Taniyama, and M. Notomi, *Applied Physics Letters* **91**, 021110 (2007), <https://doi.org/10.1063/1.2757099>.
- [15] E. Weidner, S. Combri, A. de Rossi, N.-V.-Q. Tran, and S. Cassette, *Applied Physics Letters* **90**, 101118 (2007), <https://doi.org/10.1063/1.2712502>.
- [16] L.-D. Haret, T. Tanabe, E. Kuramochi, and M. Notomi, *Opt. Express* **17**, 21108 (2009).
- [17] A. de Rossi, M. Lauritano, S. Combrié, Q. V. Tran, and C. Husko, *Phys. Rev. A* **79**, 043818 (2009).
- [18] G. Priem, P. Dumon, W. Bogaerts, D. V. Thourhout, G. Morthier, and R. Baets, *Opt. Express* **13**, 9623 (2005).
- [19] T. J. Johnson, M. Borselli, and O. Painter, *Opt. Express* **14**, 817 (2006).
- [20] W. H. P. Pernice, M. Li, and H. X. Tang, *Opt. Express* **18**, 18438 (2010).
- [21] S. Malaguti, G. Bellanca, A. de Rossi, S. Combrié, and S. Trillo, *Phys. Rev. A* **83**, 051802 (2011).
- [22] N. Cazier, X. Checoury, L.-D. Haret, and P. Boucaud, *Opt. Express* **21**, 13626 (2013).
- [23] A. M. Yacomotti, P. Monnier, F. Raineri, B. B. Bakir, C. Seassal, R. Raj, and J. A. Levenson, *Phys. Rev. Lett.* **97**, 143904 (2006).
- [24] M. Brunstein, A. M. Yacomotti, I. Sagnes, F. Raineri, L. Bigot, and A. Levenson, *Phys. Rev. A* **85**, 031803 (2012).
- [25] Y. Kuramoto, *Chemical oscillations, waves, and turbulence* (Courier Corporation, 2003).
- [26] H. Nakao, (2017), 10.1080/00107514.2015.1094987, [arXiv:1704.03293](https://arxiv.org/abs/1704.03293).
- [27] E. Kuramochi, E. Grossman, K. Nozaki, K. Takeda, A. Shinya, H. Taniyama, and M. Notomi, *Opt. Lett.* **39**, 5780 (2014).
- [28] T. Tanabe, M. Notomi, E. Kuramochi, A. Shinya, and H. Taniyama, *Nature Photonics* **1**, 49 (2007).
- [29] L. Mandel and E. Wolf, *Optical coherence and quantum optics* (Cambridge university press, 1995).
- [30] R. Loudon, *Reports on Progress in Physics* **43**, 913 (1980).
- [31] T. Van Vaerenbergh, M. Fiers, J. Dambre, and P. Bienstman, *Phys. Rev. A* **86**, 063808 (2012).
- [32] L. Zhang, Y. Fei, T. Cao, Y. Cao, Q. Xu, and S. Chen, *Phys. Rev. A* **87**, 053805 (2013).
- [33] T. Tanabe, H. Taniyama, and M. Notomi, *J. Lightwave Technol.* **26**, 1396 (2008).
- [34] In actual numerical simulations, we introduce the noise to a difference equation as $\sigma \xi_R \sqrt{dt}$, where $\sigma = 0.045\sqrt{\kappa}$ and ξ_R is a random number following the normal distribution $N(0, 1)$.
- [35] Louisell, *Quantum statistical properties of radiation*, Vol. 7 (Wiley New York, 1973).
- [36] N. G. Van Kampen, *Stochastic processes in physics and*

- chemistry*, Vol. 1 (Elsevier, 1992).
- [37] H. Risken, in *The Fokker-Planck Equation* (Springer, 1996) pp. 63–95.
 - [38] One may find that Eq. (6) is analogous to the well-known Schawlow-Townes linewidth reduction in laser physics.
 - [39] M. O. Scully and M. S. Zubairy, “Quantum optics,” (1999).
 - [40] M. Marconi, F. Raineri, A. Levenson, A. M. Yacomotti, J. Javaloyes, S. H. Pan, A. E. Amili, and Y. Fainman, “Mesoscopic limit cycles in coupled nanolasers,” (2019), arXiv:1911.10830.